Revista Facultad de Ingeniería
Universidad de Antioquia
ISSN: 0120-6230
revista.ingenieria@udea.edu.co
Universidad de Antioquia
Colombia

Restrepo-Arcila, Sandra Milena; Echavarría-Velásquez, Alejandro Iván; Giraldo Cadavid, Marco Antonio; Calderón-Gutiérrez, Jorge Andrés; Sánchez-Londoño, Héctor Darío
Colour evolution of the oxide layer formed on the Au-25Fe AND Au-24.5Fe-0.5Co
Revista Facultad de Ingeniería Universidad de Antioquia, núm. 78, marzo, 2016, pp. 62-68
Universidad de Antioquia
Medellín, Colombia

redin Revista Facultad de Ingeniería, Universidad de Antioquia, No. 78, pp. 62-68, 2016

Colour evolution of the oxide layer formed on the Au-25Fe AND Au-24.5Fe-0.5Co

Evolución del color de la capa de óxido formada en las aleaciones Au-25Fe y Au-24.5Fe-0.5Co

Sandra Milena Restrepo-Arcila[1*], Alejandro Iván Echavarría-Velásquez[1], Marco Antonio Giraldo Cadavid[2], Jorge Andrés Calderón-Gutiérrez[1], Héctor Darío Sánchez-Londoño[1]

[1]Facultad de Ingeniería, Universidad de Antioquia. Calle 67 # 53-108. A. A. 1226. Medellín, Colombia.
[2]Facultad de Ciencias Exactas y Naturales, Universidad de Antioquia. Calle 67 # 53-108. A. A. 1226. Medellín, Colombia.

ARTICLE INFO
Received July 6, 2015
Accepted January 28, 2016

KEYWORDS
Magnetite, oxide layer, coloured gold alloys, colour theory

Magnetita, capa de oxidación, aleaciones de oro coloreadas, teoría del color

ABSTRACT: The colour theory proposed by Heavens in 1991 has been applied to calculate the thickness of magnetite thin layers, Fe_3O_4, which were obtained by heat treatment at 250 °C in a gold alloy **(Au-24.5Fe-0.5Co).** The reflectance spectra obtained from the polished samples with different oxidation (and colour) degrees were used to calculate the real part of the refraction index and the (imaginary) extinction coefficients of both the metallic substrate (n_2, k_2) and the magnetite layer (n_1=2.42, k_1). The $a+b\lambda+c\lambda^2$ form was taken adjusting parameters between experimental and theoretical curves. The fitting of the data resulted in deviations between 2 and 10% for thicknesses in the range of 0 nm (only substrate) and 65 nm (dark blue colour). By means of a mathematic model and following the Heavens' theory, the thickness of each layer has been predicted with high precision, using the spectral reflectance. Consequently, we propose that by using this methodology, the values of the extinction coefficients of the oxide species can be easily obtained, and the thicknesses of the oxide layers can be predicted. The magnetite thickness values found in this study fall into the interval reported in the literature for first-order interference in steels, from light-yellow (~46 nm) to blue (~72 nm).

RESUMEN: Se aplica la teoría del color propuesta por Heavens (1991) para el cálculo de los espesores de las películas delgadas de magnetita, Fe_3O_4, los cuales fueron obtenidos por tratamiento térmico a 250°C de una aleación de oro **(Au-24.5Fe-0.5Co)**. Los espectros de reflectancia obtenidos de las muestras pulidas con diferentes grados de oxidación (y de color) fueron usados para calcular los índices de refracción (real) y de extinción (imaginario) del sustrato metálico (n_2, k_2) y de la capa de magnetita (n_1=2,42, k_1). La forma $a+b\lambda+c\lambda^2$ se tomó del ajuste de parámetros entre las curvas experimentales y teóricas. El ajuste de los datos resultan en desviaciones entre 2 y 10%, para los espesores en el rango de 0 nm (solo metal original) y 65 nm (color azul oscuro). Por medio de un modelo matemático siguiendo la teoría de Heavens, el espesor de cada capa ha sido predicho con alta precisión, utilizando las mediciones de reflectancia espectral. En consecuencia, proponemos que mediante el uso de esta metodología se pueden obtener fácilmente los valores de los coeficientes de extinción de las especies de óxido y, además, se pueden predecir los espesores de la capa de óxido. Los valores de espesores de la magnetita encontrados en la presente investigación están dentro del intervalo reportado en la literatura para la interferencia de primer orden en los aceros, desde el amarillo claro (~46 nm) hasta el azul (~72 nm).

1. Introduction

The different colours, hues, and their variation with the angle of observation that are present in metallic alloys are an innovative feature for jewellery pieces. Furthermore, in the field of optics, it is quite known that the iridescence which originates from the optical thin films would generate stunning colours that will be appreciated by jewellery lovers, just like the iridescent effect formed in soap bubbles. When iron reacts with oxygen, an iron oxide, generally magnetite, (Fe_3O_4) is formed. In a minor proportion, hematite (Fe_2O_3), can also be formed. If this oxide is generated on the appropriate substrate, that is, one with sufficient iron, a layer of magnetite will cover the substrate. It is expected that the thickness of such layer will be dependent on the method applied to obtain the oxide. Iron oxides can be obtained in three ways: thermically (and then called *frosted),*

*Corresponding author: Sandra Milena Restrepo Arcila
e-mail: sandra.restrepoa@udea.edu.co
ISSN 0120-6230
e-ISSN 2422-2844

DOI: 10.17533/udea.redin.n78a08

chemically or electrochemically. The later, anodically oxidized in the presence of alkali [1] Table1, Figure 1.

Table 1 Comparative list of layer thicknesses for two types of oxides; Fe_3O_4 and SiO_2. The Fe_3O_4 layers were obtained by anodic oxidation formed on steel (SAE 1010) with 1 minute increments in a solution of 50% KOH at 70°C and +2 V vs. steel counter electrode [1].

Colour	(SAE 1010) Fe_3O_4	SiO_2
Brown	40 nm	70 nm
Dark violet	60 nm	100 nm
Red violet	160 nm	270 nm
Blue	180 nm	300 nm

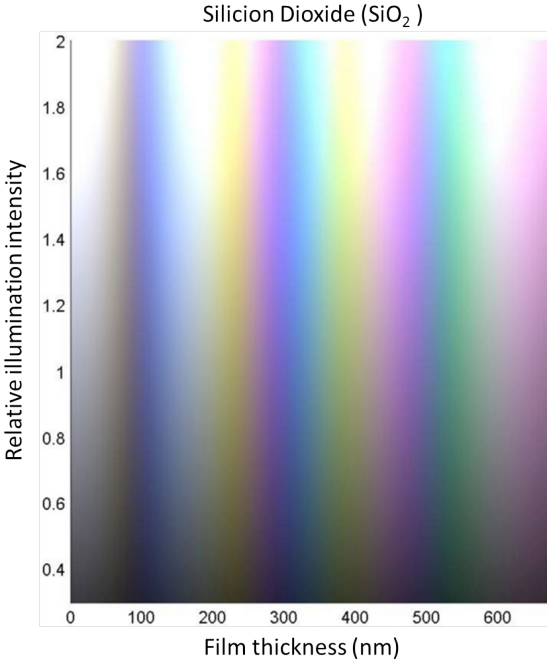

Figure 1 Silica reference taken from [2]

This oxide layer filters light waves by reflection, producing brilliant colours. As the thickness of the oxide layer changes, so does its colour and appearance, producing outstanding iridescence.

Magnetite is black when observed in a bulk, but when forming a thin layer it is blueish. Hematite, on the other hand, shows a reddish-brown colour. For steel, the reported content of hematite is about a 5% of the total oxide, and a 95% of magnetite [3, 4].

The following thicknesses for first-order interference colours in iron oxide layers [5]: pale yellow, 46 nm; reddish yellow, 52 nm; reddish brown, 58 nm; purple, 63 nm; violet, 68 nm; and blue, 72 nm. As the thickness grows, a reduction of glow is observed. A similar colour range is observed in other types of material layers formed by oxidation, such as TiO_2, SiO_2 and Si_3N_4 among others [5].
Colour variation can also be obtained by oxidation on a steel surface when the steel is heated at temperatures between 180°C and 427°C [6]. A typical colour scale is shown in Figure 2.

Figure 2 (a) Steel quenching colours according to temperature treatment and (b) photography of an actual piece of steel. Taken from [6]

Several heat treatments have been reported on different alloys. There is a patent concerning the production of intense blue coloured layers on a **Au-24,5Fe-0,5Ni** alloy, when treated at 450-600 °C between 10 and 15 minutes [7]. Also patented a treatment to produce iridescent blue on AuCrMoVCWFe alloys after a rather rapid treatment with flame [8, 9].

The aim of this study is to numerically determine the thicknesses of iron oxide thin films formed by heat treatment of the **Au-24.5Fe-0.5Co** alloy and their relationship with the measured colour by spectrophotometrical methods.

2. Experimental procedure

2.1. Alloy preparation

Refined gold was obtained by *quartering* and subsequent dissolution in nitric acid, HNO_3, (following ASTM E 1335 norm, method A) [10]. Iron (analytic grade) was purchased from *J.J Baker Chemical Co* (99.95% purity) and cobalt (micronized) was commercially obtained from *Goodfellow Cambridge* Ltd. (99.95% purity). Graphite crucibles coated with zirconia were used to avoid iron or cobalt contamination. Alloys were melted in a BEGO induction

(a) (b)

Figure 3 (a) BEGO induction furnace in argon atmosphere. (b) Actual photograph of the furnace arm.

furnace in presence of an Argon inert atmosphere to avoid iron and cobalt oxidation during the process (Figure 3).

The melted components were then centrifuged in the furnace and deposited in a metal mold of 5mm diameter and approximately 15 mm long. Afterwards, the piece was sectioned in five smaller pieces of about 3 mm length. Each cylinder was deformed by cold compression (at 140 ksi), until reducing their length to 0.5 mm. This procedure allowed us to evaluate their mechanical resistance. The samples were then gently polished until obtaining a mirror finishing. The final colours of the samples corresponding to the oxide layers were subsequently obtained by air heating in an electric furnace at constant 250 °C between 5 and 60 minutes of sustainability, in which yellow-brown, pink, violet, purple and intense blue hues (as observed with the naked eye) were obtained.

2.2. Surface characterization

A bifurcated probe of 200 µm diameter was used (*Avantes* optical fiber probe) to measure reflectance spectra of the metallic alloy samples with normal incidence. The probe was held on a micromanipulator with three degrees of freedom (3D movement) to be able to measure and compare different areas of the samples. A halogen and deuterium double light source was used (*Avalight*-DH-S-BAL) for deep UV and visible range respectively. Reflected light was captured and taken to an *Avantes* spectrophotometer (*AvaSpec*-2048). A first surface mirror was used as calibration standard.

The reflectance spectra obtained were normalized. The calculations of the thicknesses were made according to the colour theory proposed by Heavens [12]. The real part of the refraction index and the (imaginary) extinction coefficient of the metallic substrate (n_2, k_2) and the oxide layers (n_1, k_1) in the $\boldsymbol{a+b\lambda+c\lambda^2}$ form were taken as adjusting parameters between experimental and theoretical curves. A fitting of the data with deviations between 2% and 10% for 0 nm (only substrate) and 61 nm (dark blue colour) thicknesses were found. The surfaces of the alloys were also characterized by micro-Raman spectroscopy by using a confocal Raman spectrometer (*Horiba Jobin Yvon*, model *Labram* HR). A laser He/Ne of 632 nm was used. The zones for micro-Raman analysis were observed using a Nikon BX41 focal microscope with plan achromatic objectives.

3. Results and analysis

Depending on the time of heat treatment applied to the Au alloy samples, different colours were obtained, ranging from ochre yellow (minimum time) to black (maximum time), through fuchsia, purple and blue. The thickness of the layers formed on the samples are so thin that it is impossible to measure them directly; therefore, colour theory is usually applied. Here, we have used the theory proposed by Heavens [12] to calculate the thickness of each oxide layer to ultimately being able to predict the colour of a given oxidation time. Two alloys were then treated as referred in section 2.1 (**Au-24.5Fe-0.5Co** and **Au-25Fe**, at 250°C, for a series of times). In this case, reflectance equations are deduced from the scheme shown in Figure 4.

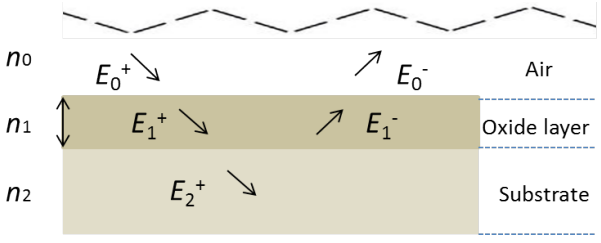

Figure 4 Schematic representation of an absorbing layer in an absorbing substrate. The upper medium is air

The amplitude of incident and reflected waves are considered to be a function of *Fresnell* coefficients, r_1 and r_2, which correspond to the oxide layer and the metallic substrate, respectively. We reserve r_0 for air.

The resulting equations are presented as follows (Eqs. 1 and 2):

$$\begin{pmatrix} E_0^+ \\ E_0^- \end{pmatrix} = \left(\frac{1}{t_1}\right)\begin{pmatrix} 1 & r_1 \\ r_1 & 1 \end{pmatrix}\begin{pmatrix} E_1^+ \\ E_1^- \end{pmatrix} \quad (1)$$

$$\begin{pmatrix} E_1^+ \\ E_1^- \end{pmatrix} = \left(\frac{1}{t_2}\right)\begin{pmatrix} e^{i.\delta_1} & r_2 e^{i.\delta_1} \\ r_2 e^{-i.\delta_1} & e^{-i.\delta_1} \end{pmatrix}\begin{pmatrix} E_2^+ \\ E_2^- = 0 \end{pmatrix} \quad (2)$$

E_0^+, E_1^+, E_2^+ are the amplitudes of the electric vectors of the incident (or transmitted) waves in the layers 1, 2 and 3. E_0^-, E_1^-, E_2^- the amplitudes of the electric vectors of the waves reflected on the layers 1, 2, 3 (here, $E_2^- = 0$).

n_0, n_1, n_2 are the complex refraction indices of layers 1, 2 and 3 ($n_m = n_m - ik_m$, with $k_0 = 0$)

r_1, r_2 are the Fresnel reflection coefficients of the light traveling through the layers 0→1 and 1→2 expressed as: $r_m = g_m + ih_m$ in Eq. (3).

$$r_m = g_m + ih_m \equiv \frac{n_{m-1} - n_m}{n_{m-1} + n_m} \quad (3)$$

In r_1 and r_2 cases, real and imaginary coefficients are showed in Eqs. (4-7):

$$g_1 = \frac{n_0^2 - n_1^2 + k_1^2}{(n_0 + n_1)^2 + (k_1)^2} \quad (4)$$

$$h_1 = \frac{2(n_0 k_1)}{(n_0 + n_1)^2 + (k_1)^2} \quad (5)$$

$$g_2 = \frac{n_1^2 - n_2^2 + k_1^2 - k_2^2}{(n_1 + n_2)^2 + (k_1 + k_2)^2} \quad (6)$$

$$h_2 = \frac{2(n_1 k_2 - n_2 k_1)}{(n_1 + n_2)^2 + (k_1 + k_2)^2} \quad (7)$$

Replacing (2) in (1), we have the Eq. (8):

$$\begin{pmatrix} E_0^+ \\ E_0^- \end{pmatrix} = \left(\frac{1}{t_1 t_2}\right)\begin{pmatrix} 1 & r_1 \\ r_1 & 1 \end{pmatrix}\begin{pmatrix} e^{i.\delta_1} & r_2 e^{i.\delta_1} \\ r_2 e^{-i.\delta_1} & e^{-i.\delta_1} \end{pmatrix}\begin{pmatrix} E_2^+ \\ E_2^- = 0 \end{pmatrix} \quad (8)$$

and by matrix product in Eqs. (9-12), it reduces to:

$$\begin{pmatrix} E_0^+ \\ E_0^- \end{pmatrix} = \left(\frac{1}{t_1 t_2}\right)\begin{pmatrix} e^{i.\delta_1} + r_1 r_2 e^{-i.\delta_1} & r_2 e^{i.\delta_1} + r_1 e^{-i.\delta_1} \\ r_1 e^{i.\delta_1} + r_2 e^{-i.\delta_1} & r_2 e^{i.\delta_1} + e^{-i.\delta_1} \end{pmatrix}\begin{pmatrix} E_2^+ \\ E_2^- = 0 \end{pmatrix} \quad (9)$$

$$\begin{pmatrix} E_0^+ \\ E_0^- \end{pmatrix} = \left(\frac{1}{t_1 t_2}\right)\begin{pmatrix} e^{i.\delta_1} + r_1 r_2 e^{-i.\delta_1} \\ r_1 e^{i.\delta_1} + r_2 e^{-i.\delta_1} \end{pmatrix}(E_2^+) \quad (10)$$

$$E_0^- = \frac{E_2^+}{t_1 t_2}\left(r_1 e^{i.\delta_1} + r_2 e^{-i.\delta_1}\right) \quad (11)$$

$$E_0^+ = \frac{E_2^+}{t_1 t_2}\left(e^{i.\delta_1} + r_1 r_2 e^{-i.\delta_1}\right) \quad (12)$$

Reflectance is defined in Eq. (13), as:

$$R = \frac{E_0^-}{E_0^+} = \frac{r_1 e^{i.\delta_1} + r_2 e^{-i.\delta_1}}{e^{i.\delta_1} + r_1 r_2 e^{-i.\delta_1}} \quad (13)$$

In terms of energy of the reflected waves vs. incident in Eqs. (14-20):

$$\boldsymbol{R} = \frac{E_0^- E_0^{-*}}{E_0^+ E_0^{+*}} = \frac{\left(r_1 e^{i.\delta_1} + r_2 e^{-i.\delta_1}\right)^2}{\left(e^{i.\delta_1} + r_1 r_2 e^{-i.\delta_1}\right)^2} \quad (14)$$

$$\boldsymbol{R} = \frac{\left((g_1 + ih_1)\left(e^{\alpha_1}(cos\gamma_1 + isen\gamma_1)\right) + (g_2 + ih_2)\right)}{\left(\left(e^{\alpha_1}(cos\gamma_1 + isen\gamma_1)\right) + (g_1 + ih_1)(g_2 + ih_{m2})\right)}$$

$$\frac{\left(e^{-\alpha_1}(cos\gamma_1 - isen\gamma_1)\right)^2}{\left(e^{-\alpha_1}(cos\gamma_1 - isen\gamma_1)\right)^2} \quad (15)$$

$$\boldsymbol{R} = \frac{(g_1^2 + h_1^2)e^{2\alpha_1} + (g_2^2 + h_2^2)e^{-2\alpha_1} + Acos2\gamma_1 + Bsen2\gamma_1}{e^{2\alpha_1} + (g_1^2 + h_1^2)(g_2^2 + h_2^2)e^{-2\alpha_1} + Ccos2\gamma_1 + Dsen2\gamma_1} \quad (16)$$

$$A = 2(g_1 g_2 + h_1 h_2) \quad (17)$$

$$B = 2(g_1 h_2 - g_2 h_1) \quad (18)$$

$$C = 2(g_1 g_2 - h_1 h_2) \quad (19)$$

$$D = 2(g_1 h_2 + g_2 h_1) \quad (20)$$

n_2, k_2 parameter adjustments were made modeling the experimental with the theoretical result, under the presumption d=0 (without magnetite layer), resulting in Eqs. (21) and (22):

$$n_2 = 5.408 - 0.01209\lambda + 1.049e^{-5} * \lambda^2 \quad (21)$$

$$k_2 = 4.2970 - 0.01419\lambda + 2.760e^{-5} * \lambda^2 \quad (22)$$

Previous equations show the tendency presented in Figure 5.

Figure 6 shows the reflectance curve measured in the spectrophotometer with modeling adjustment (1.7%) for Au-24.5Fe-0.5Co alloy without superficial oxide layer.

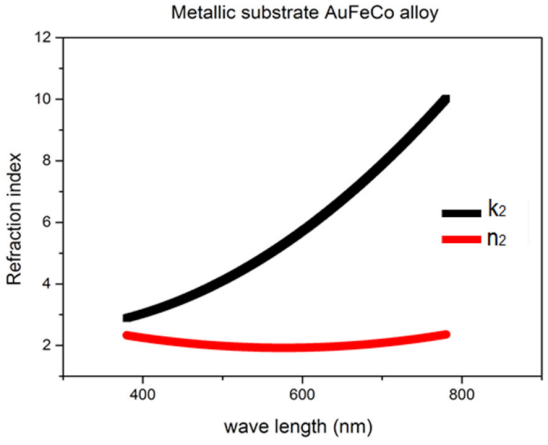

Figure 5 Calculated values of the substrate coefficients, n_2 and k_2 obtained from the applied model. The reflectance spectra were experimentally measured and included in Eqs. (21) and (22)

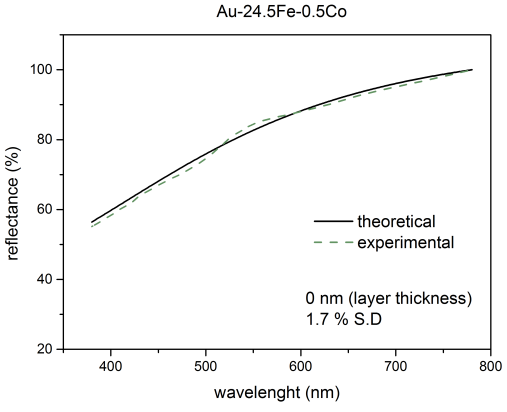

Figure 6 Comparison between experimental and theoretical reflectance spectra (with 1.7% standard deviation) for a layer thickness of 0 nm

Once the constant parameters, n_1 and k_1, of the substrate were obtained, their values were introduced in the model to calculate the oxide layer parameters, n_{-1} and k_{-1}. The obtained value for the real part (n_2 = 2.48 in Eq. (23)) is in remarkably good agreement with that reported in reference [4] (n between 2.42 and 3.0 for oxides with concentrations around 95% magnetite). The extinction coefficient, k_1, is, according to Eq. (24):

$$n_1 = 2.48 \quad (23) \tag{23}$$

$$k_1 = 0.6609 - 0.00000 - 1.288e^{-5} * \lambda^2 \quad (24) \tag{24}$$

Figure 7 shows the extinction coefficients of the magnetite formed in air-oxidation of the alloys **Au-24.5Fe-0.5Co** and carbon steel [13].

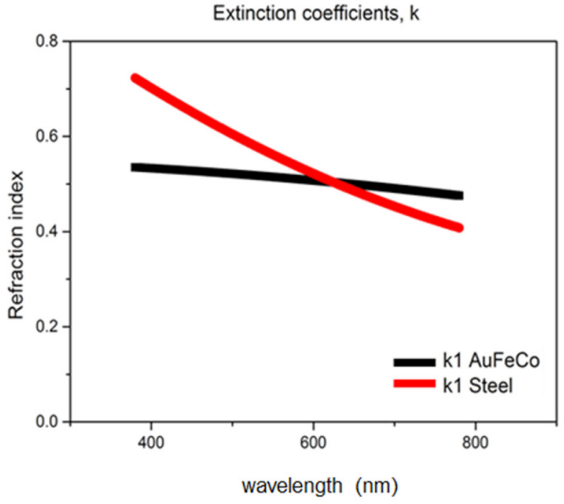

Figure 7 Extinction coefficients for the magnetite formed by oxidation of the alloys AuFeCo and carbon steel

Different thickness results for coloured samples at different times of heat treatments (250°C) are shown in Figure 8 (a, b, c, d).

The calculated thickness values obtained after heat treatment were compared with those reported by other authors [13] who obtained a magnetite layer in low carbon steels. According to our results in a gold alloy, a magnetite thin layer appeared after heat treatment. However, regarding the results shown in Figure 7, it can be seen that the values of the extinction coefficient are slightly different, probably because the base alloys are different. It must be highlighted that this author obtained the blue colour with a thickness of 98 nm (in carbon steel), whilst we obtained the same colour with 61 nm (in gold alloy).

The oxide thickness values that were found in this study fall in the interval reported for first-order interference in steels, from light yellow (46 nm) to blue (72 nm) [1, 2, 13].

In order to determine the type of oxide that constitutes the film, we performed *Raman* spectroscopy of all our samples.

Figure 9 shows the *Raman* spectra of the sample surfaces after heat treatment. As a confirmation of our expectations, all the spectra show the characteristic peak of magnetite (Fe_3O_4) near to 700 cm^{-1} in both alloy systems. Furthermore, the presence of hematite (Fe_2O_3) is also observed, because of the pair of bands near to 400 and 1500 cm^{-1}. The difference in proportion between magnetite and hematite is evident from the very different intensity of the peaks, as already reported in the literature [3, 4]. Such behavior is observed in all the samples analyzed. On the other hand, regarding the analysis of the time of oxidation compared to the composition, we observed that the samples with a longer treatment corresponded to the highest spectra. In general, the higher the spectra, the longer the time.

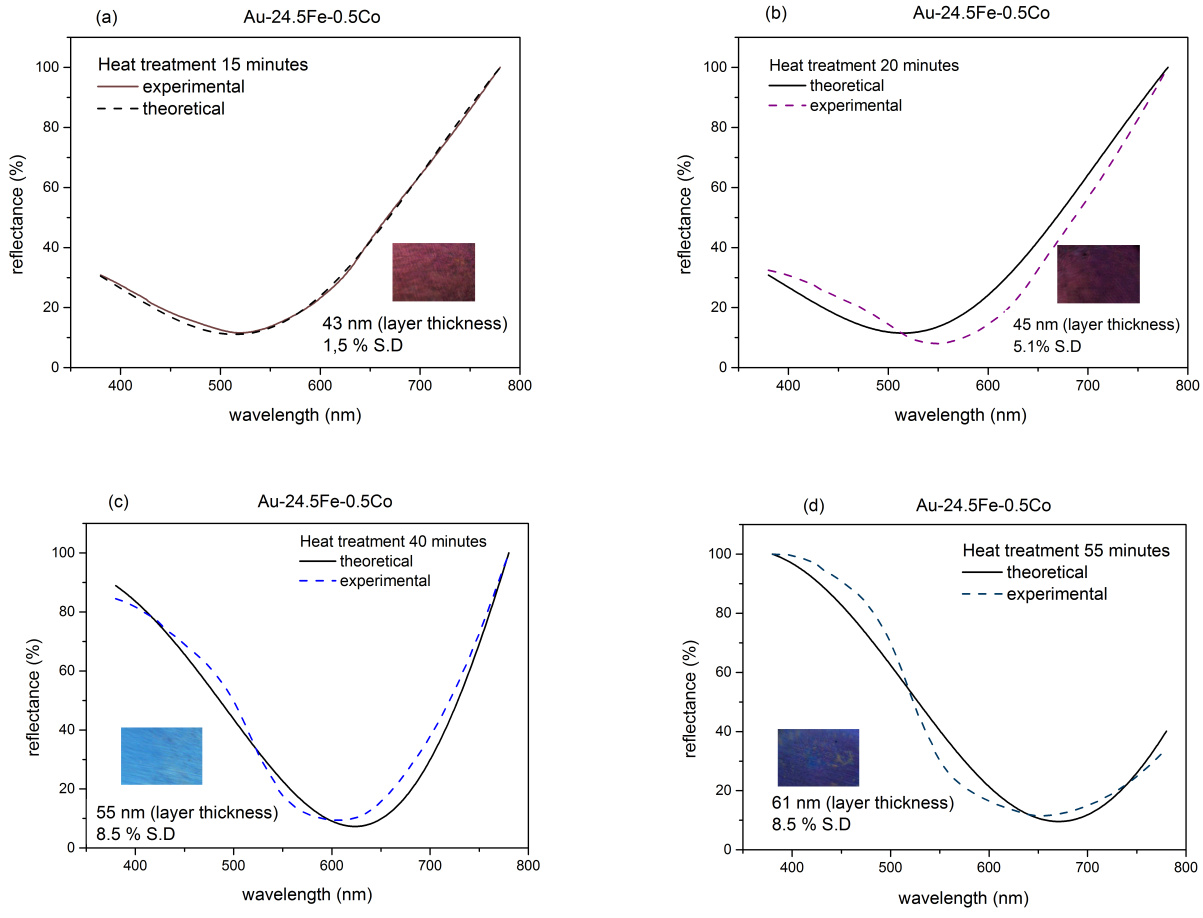

Figure 8 Photographs of the coloured oxides for the studied alloys with their corresponding reflectance curves

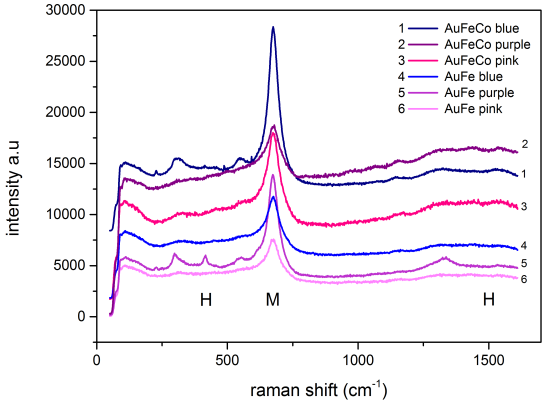

Figure 9 Raman spectra for the Au-25Fe and the Au-24.5Fe-0.5Co alloy systems, M: magnetite, H: hematite. The treatment was at a constant temperature of 250°C, for times between 5 and 60 minutes

4. Conclusions

The colour of both gold alloys is produced by the formation of a fine layer of superficial iron oxide (composed by magnetite and hematite). We have shown by using spectrophotometrical and material composition analyses that the colour of the alloys strongly rely on the thickness of the iron oxide layer, which will depend on the time of treatment. We have created oxide layers with colors that range from yellow (20 nm) to blue (61 nm) that are composed by –mostly– magnetite and also hematite.

In addition to the reported experimental analyses, we performed a theoretical study of the colours created by the thin layers formed when the alloys were put under heat treatment. Until now, the physical model described by Heavens was used only for low carbon-steel. We applied the theory to two distinct alloy systems and demonstrated its validity. Moreover, we were able to calculate the extinction coefficients for the substrates and for the layers by experimentally measuring the reflectance spectra of the samples. To our knowledge, this is the first time that these

values are reported for gold alloys. We propose this method to be applied for any substrate in which colouration will be a result of an oxide layer plus the base colour of the alloy. Thus, the possibilities are very diverse in jewelry design.

5. Acknowledgments

We thank to CIDEMAT, GIPIMME and BIOPHYSICS research groups. We also thank the program "average academic scholarship stimulus" of Vicerrectoría de Docencia de la Universidad de Antioquia.

This project was partially funded by "Estrategia de Sostenibilidad 2014-2015 de la Universidad de Antioquia".

6. References

1. T. Burleigh *et al.*, "Anodizing Steel in KOH and NaOH Solutions", Journal of The Electrochemical Society, vol. 154, no. 10, pp. 579-586, 2007.
2. Brigham Young University, *Silicon Dioxide SiO_2*. [Online]. Available: http://www.cleanroom.byu.edu/color_chart.parts/sio2_chart.jpg. Agosto 2013. Accessed on: Aug. 1, 2013.
3. Finishing Industry ®, *Questions regarding chemical reaction that occurs when Bluing Steel*, 2007. [Online]. Available: http://www.finishing.com/453/44.shtml. Accessed on: Feb. 1, 2013.
4. Ether (Atmospheric Chemistry Data Centre), *Real and imaginary indices of refraction of hematite particles at T=293 K.* [Online]. Available: http://ether.ipsl.jussieu.fr/ether/pubipsl/aerosols/massie2000/hematiteT293.longtin. Accessed on: Jan. 1, 2013.
5. F. Constable, "Spectrophotometric Observations on the Growth of Oxide Films on Iron, Nickel, and Copper" *Roy. Soc. Proc., A*, vol. 117, pp. 376-387, 1928.
6. Simply Tool Steel, *Temperature Color Guide*. [Online]. Available: http://www.simplytoolsteel.com/temperature-color-guide.html. Accessed on: Jul. 1, 2013
7. L. Muller, "Coloring a gold alloy", U.S. Patent 5 059 255 A, Oct. 22, 1991.
8. C. Cretu and E. Van der Lingen, "Coloured gold alloys", *Gold Bulletin*, vol. 32, no. 4, pp. 115-126, 1999.
9. V. Antoniazzi, "Goldlegierung mit irisierender, blaeulicher farbe, verfahren zu ihrer herstellung und ihre verwendung", DE Patent 3 641 228, Dec. 3, 1986.
10. American Society for Testing Materials (ASTM International), *Standard Test Methods for Determination of Gold in Bullion by Fire Assay Cupellation Analysis*, ASTM Standard E1335-08, 2008.
11. IndiaMART, *Induction Casting Machine Bego (fornax)* [Online]. Available: http://trade.indiamart.com/details.mp?offer=7822509212. Accessed on: Jun. 1, 2013.
12. O. Heavens, *Optical properties of thin solid films*, 1st ed., New York, USA: Dover Pub., Inc., 1991.
13. Y. Fujimura, "Numericalization of the temper color by the oxide film thickness", *Journal of the Japan Society of Precision Engineering*, vol. 38, no. 454, pp. 902-907, 1972.